$Me_4C_5CH_2CH_2C_5Me_4)[RhCl_2]$, 120906-04-9; PMe_3, 594-09-2; $[WH_5(PMe_3)](\eta^5,\eta^5$-$Me_4C_5CH_2CH_2C_5Me_4)\{[RhMe(CO)(PMe_3)][O_3SCF_3]\}$, 120906-06-1; $[FeCp_2][PF_6]$, 11077-24-0; $Co_2(CO)_8$, 10210-68-1; $WCp^*Me(CO)_3$, 34807-90-4; $W(CO)_6$, 14040-11-0; $[WMe(CO)_3](\eta^5$-$Me_4C_5CH_2CH_2C{\equiv}CMe)$, 120906-07-2; $[WCl_4(PMe_3)](\eta^5,\eta^5$-$Me_4C_5CH_2CH_2C_5Me_4)[WMe(CO)_3]$, 120906-08-3; $[WCl_4]_2(\eta^5,\eta^5$-$Me_4C_5CH_2CH_2C_5Me_4)$, 120906-09-4; $[WMe_4]_2(\eta^5,\eta^5$-$Me_4C_5CH_2CH_2C_5Me_4)$, 120906-10-7.

Contribution from the Department of Chemistry,
The Ohio State University, Columbus, Ohio 43210

Electronic Structure of Piano-Stool Dimers. 8. Electronically Induced Conformational Changes in High-Valent Bimetallic Chalcogen Complexes of the Type $[CpML]_2(\mu$-$L)_2$ (M = Mo, Re; L = S, O)[1]

Bruce E. Bursten*,[2] and Roger H. Cayton

Received February 17, 1988

Fenske-Hall molecular orbital calculations have been applied to a series of bimetallic chalcogen complexes that adhere to the general formula $Cp_2M_2L_4$, where M = Mo, Re and L = O, S. In the case of M = Mo and L = S three geometric isomers were considered: $[CpMoS]_2(\mu$-$S)_2$ (**1**), $[CpMo]_2(\mu$-$S)_2(\mu$-$S_2)$ (**2**), and $[CpMoS]_2(\mu$-$S_2)$ (**3**). Series of calculations were performed in order to create a potential surface modeling an isomerization pathway among the three isomers. It was found that the conversion from **1** to **2** is a photochemically allowed process, whereas the conversion from **2** to **3** is allowed thermally. In the related oxo compound $[CpMoO]_2(\mu$-$O)_2$ (**4**), the reason for the puckering of the central Mo_2O_2 core was found to be due to a more favorable Mo-(μ-O) π interaction in the slightly folded geometry. In addition, folding the μ-oxo ligands of **4** toward the cis Cp rings, rather than away from the Cp rings in a sterically less congested environment, was found to be the electronically preferred geometry. Further puckering of the μ-oxo ligands of **4** to form a μ-peroxo structure was calculated to be a significantly higher energy process than the same distortion coordinate associated with the sulfide analogue. Calculations on the d^2-d^2 complex $[CpReO]_2(\mu$-$O)_2$ (**5**) at Re-Re distances varying from 2.74 to 3.54 Å indicate the most stable configuration to be at 3.14 Å. This stable geometry at 3.14 Å appears to be the result of the generation of two nonbonding, Re-based orbitals that are then able to hold the four metal-based electrons. At both longer and shorter Re-Re distances, the μ-oxo ligands destabilize one of the two nonbonding orbitals to generate a high-energy HOMO.

Discrete bimetallic organotransition-metal chalcogen complexes have recently been the subject of extensive research. Compounds of this type represent a link between ionic, solid-state metal chalcogenides and low-valent organometallic systems. Of particular interest are sulfur-containing species of this type that serve as models for heterogeneous desulfurization catalysts used in the purification of petroleum products.[3,4] An interesting series of bimetallic chalcogen complexes is that which adheres to the general formula $(\eta^5$-$C_5R_5)_2M_2L_4$, where L = O, S. Crystallographically characterized members of this high-valent piano-stool dimer series have been prepared for a variety of transition metals including V,[5] Cr,[6] Mo,[7-11] Re,[12] Fe,[13,14] and Co.[14] Not surprisingly, the structures of these compounds are highly dependent upon the oxidation state and corresponding electronic requirements of the metal. Moreover, even within the series of Mo complexes where L = S, three different structure types have been observed, viz. $[Cp^*MoS]_2(\mu$-$S)_2$ (**1**), $[Cp^*Mo]_2(\mu$-$S)_2(\mu$-$S_2)$ (**2**), and $[Cp^*MoS]_2(\mu$-$S_2)$ (**3**) ($Cp^* = \eta^5$-C_5Me_5), two of which (**1**, **2**) have been characterized crystallographically.[10,11] These three isomers are illustrated in A. The chemistry of these species is also relevant

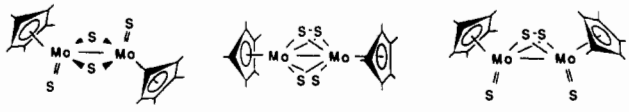

1 **2** **3**

A

to the understanding of the coordination of sulfur ligands to molybdenum in biological systems.[15,16] The tetraoxo analogues of this system are also known for the metals Cr, Mo, and Re, and in each case their structures resemble the basic structure of **1**. To date, there has been no evidence for peroxo analogues of structure types **2** and **3** in the piano-stool dimer class.

Because this series of compounds displays such a plethora of structure types and alternating metal d counts, and because of its close relationship to important heterogeneous and homogeneous systems, the need for a thorough understanding of the electronic structure and bonding operating within this system is obvious. We have found previously, in calculational treatments of piano-stool dimers containing π-acid ligands, that the Fenske-Hall method provides reliable results for such complexes and can be used to explain certain anomalous reactivity patterns as well as conformational preferences in these low-valent systems.[1,17,18] In this contribution we have extended this approach to include the high-valent bimetallic series $Cp_2M_2L_4$, where M = Mo, L = S, O and M = Re, L = O. These results will be used to examine

(1) Part 7: Bursten, B. E.; Cayton, R. H. *Polyhedron* **1988**, *7*, 943-954.
(2) Camille and Henry Dreyfus Foundation Teacher-Scholar (1984-1989).
(3) Massoth, F. E. *Adv. Catal.* **1978**, *27*, 265 and references therein.
(4) Schuman, S. C.; Shalit, H. *Catal. Rev.* **1970**, *4*, 245.
(5) Bolinger, C. M.; Rauchfuss, T. B.; Rheingold, A. L. *J. Am. Chem. Soc.* **1983**, *105*, 6321-6323.
(6) Heberhold, M.; Kremnitz, W.; Razavi, A.; Schollhorn, H.; Thewalt, U. *Angew. Chem.* **1985**, *97*, 603-604; *Angew. Chem., Int. Ed. Engl.* **1985**, *24*, 601-602.
(7) Couldwell, C.; Prout, K. *Acta Crystallogr.* **1978**, *B34*, 933-934.
(8) Arzoumanian, H.; Baldy, A.; Pierrot, M.; Petrignani, J.-F. *J. Organomet. Chem.* **1985**, *294*, 327-331.
(9) Stevenson, D. L.; Dahl, L. F. *J. Am. Chem. Soc.* **1967**, *89*, 3721-3726.
(10) Brunner, H.; Meier, W.; Wachter, J.; Guggolz, E.; Zahn, T.; Ziegler, M. L. *Organometallics* **1982**, *1*, 1107-1113.
(11) DuBois, M. R.; DuBois, D. L.; VanDerveer, M. C.; Haltiwanger, R. C. *Inorg. Chem.* **1981**, *20*, 3064-3071.
(12) Herrmann, W. A. Personal communication.
(13) Weberg, R.; Haltiwanger, R. C.; DuBois, M. R. *Organometallics* **1985**, *4*, 1315-1318.
(14) Brunner, H.; Janietz, N.; Meier, W.; Sergeson, G.; Wachter, J.; Zahn, T.; Ziegler, M. L. *Angew. Chem., Int. Ed. Engl.* **1985**, *24*, 1060-1061.
(15) Coughlan, M. P., Ed. *Molybdenum and Molybdenum-Containing Enzymes*; Pergamon Press: New York, 1980.
(16) Newton, W. C., Otsuka, S., Eds. *Molybdenum Chemistry of Biological Significance*; Plenum Press: New York, 1980.
(17) Bursten, B. E.; Cayton, R. H. *Organometallics* **1988**, *7*, 1342-1348.
(18) (a) Bursten, B. E.; Cayton, R. H. *J. Am. Chem. Soc.* **1987**, *109*, 6053-6059. (b) Bursten, B. E.; Cayton, R. H. *J. Am. Chem. Soc.* **1986**, *108*, 8241-8249 and references therein.

0020-1669/89/1328-2846$01.50/0

Scheme I

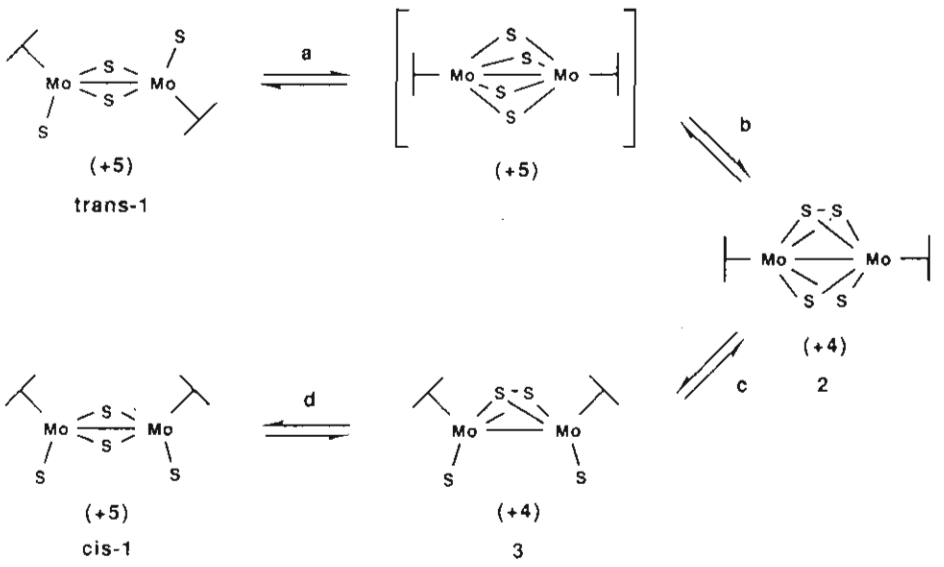

the close relationship that exists between the electronic requirements of the metals and the conformational flexibility of the various ligand sets.

$Cp_2Mo_2S_4$

Interest in the electronic structure of isomers of $Cp_2Mo_2S_4$ is not new. For example, DuBois et al. utilized EHMO calculations to investigate the bonding in $Cp_2Mo_2S_4$ (Cp = η^5-C_5H_5) in a geometry analogous to **1**, and in the as yet unobserved geometry $[CpMo]_2(\mu\text{-}S)_4$.[11,19] These calculations were primarily used to explain the preference for the tetrabridged geometry when two or more of the sulfido ligands are transformed into thiolate ligands. Previous Fenske–Hall calculations have also been applied to the sulfido complex **1**, as well as the mixed oxo–sulfido complex $[CpMoO]_2(\mu\text{-}S)_2$,[9] but only to speculate on the electrochemical properties of these compounds with respect to the structurally similar dithiolato system $[(S_2C_2H_4)MoS]_2(\mu\text{-}S)_2^{2-}$.[20] More recently, Tyler et al. applied the Xα–SW method to isomer **1** in an effort to understand its photoisomerization to geometries **2** and **3**.[21,22] Finally, Newsam et al. studied the folding of the Mo–(μ-S)–Mo bridge planes of *cis*-**1** using interactive molecular graphics.[23]

In addition to the obvious aesthetic attraction of the various isomers of $Cp^*_2Mo_2S_4$, our interest in the electronic structure and bonding operating within this unique system was further piqued by the experimentally observed thermal and photochemical interconversions among the three species. For example, Wachter et al. demonstrated that heating a toluene solution of $Cp^*_2Mo_2(CO)_4$ with elemental sulfur at 45 °C for 22 h gave only isomers **2** and **3**.[10] Longer reaction times (3 days) yielded exclusively isomers **1** and **3**. In addition, isomer **2** could be converted to **3** upon thermolysis. Furthermore, Tyler et al. have shown that irradiation of any one of the pure compounds **1**, **2**, or **3** ($\lambda < 450$ nm) eventually yields a mixture of all three isomers.[22]

One possible interconversion pathway for these isomers is depicted in Scheme I. The formal oxidation state of the metal centers is indicated below each species. This isomerization pathway involves a minimum of ligand motion during each step. This is an important point, since we wanted to examine not only the electronic structures of the various isomers but also the potential surface equilibrating them. Such an analysis will aid in understanding the isomerization behavior as well as providing insight into the reactivity of the system.

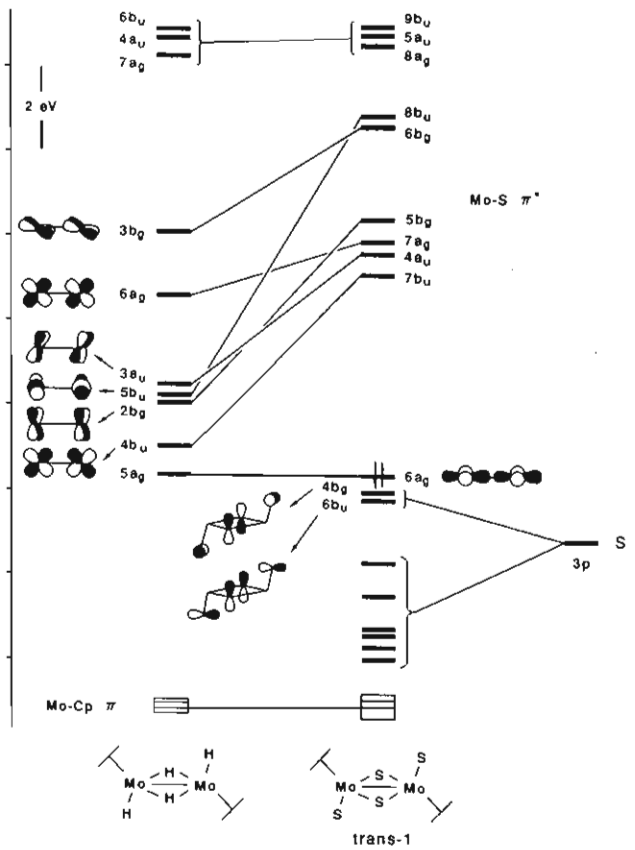

Figure 1. Frontier MO diagram of *trans*-**1** showing its correlation to the orbitals of the σ-only framework *trans*-$[CpMoH]_2(\mu\text{-}H)_2$.

Steps a, b, and c of Scheme I are meant to represent the observed photochemical isomerization among structures **1**, **2**, and **3**. Step c also represents the known thermal transformation from isomer **2** to **3**. The final step, d, was included in order to complete the cycle from *trans*-**1** to *cis*-**1**, although the cis isomer has yet to be observed for this particular ligand set. The inclusion of an electronic description of step d will also prove useful when we examine the bonding in the tetraoxo analogues. For computational purposes, the Cp* ligands of the species in Scheme I have been modeled with Cp ligands.

We will begin the analysis by deriving the frontier orbitals of the *trans*-**1** isomer. We have found previously that a convenient method for such an orbital derivation can be accomplished through

(19) DuBois, D. L.; Miller, W. K.; DuBois, M. R. *J. Am. Chem. Soc.* **1981**, *103*, 3429–3436.
(20) Szterenberg, L.; Jezowska-Trzebiatowska, B. *Inorg. Chim. Acta* **1982**, *59*, 141–145.
(21) Bruce, M. R. M.; Bruce, A. E.; Tyler, D. R. *Polyhedron* **1985**, *4*, 2073–2086.
(22) Bruce, A. E.; Tyler, D. R. *Inorg. Chem.* **1984**, *23*, 3433–3434.
(23) Newsam, J. M.; Halbert, T. R. *Inorg. Chem.* **1985**, *24*, 491–494.

prior construction of a "σ-only" bimetallic framework.[1,17,24] In addition, the pseudooctahedral environments of the metal centers in *trans*-**1** are ideally suited for this method. The frontier MO diagram of *trans*-**1** is shown in Figure 1, along with its correlation to the orbitals of the fictitious σ-only framework $[CpMoH]_2(\mu\text{-}H)_2$. The derivation of the orbitals of this type of σ-only framework has been described elsewhere[1,17,24] and hence will not be discussed further here. Orbitals $5a_g$–$6a_g$ of the σ-only framework can be thought of as a set of six "pseudo-t_{2g}" metal–ligand nonbonding orbitals resulting from the dimerization of two monomeric fragments. The lower three orbitals ($5a_g$, $4b_u$, $2b_g$) are Mo–Mo bonding, and the upper three orbitals ($5b_u$, $3a_u$, $6a_g$) are Mo–Mo antibonding in character. All six are essentially Mo–H nonbonding since the hydride ligands lack any π-type orbitals. The four orbitals highest in energy are derived from the "pseudo-e_g" sets of two monomeric fragments. Three of these ($7a_g$, $4a_u$, $6b_u$) are Mo–H antibonding, and one ($3b_g$) is Mo–H nonbonding and thus stabilized near the "pseudo-t_{2g}" set in energy. Replacement of the four hydride ligands with sulfido ligands serves to "turn on" the π-donor effects. The eight π orbitals of the sulfido ligands transform as $1a_g + 1a_u + 3b_g + 3b_u$ under C_{2h} symmetry. The nonbonding metal-based orbitals of the σ-only framework transform as $2a_g + 1a_u + 2b_g + 2b_u$; hence, a metal-based a_g orbital and two ligand-based orbitals (b_g and b_u) are left without symmetry matches and thus remain nonbonding. The two ligand-based orbitals, $6b_u$ and $4b_g$, ultimately lie close in energy to the metal-based $6a_g$ orbital. The $6a_g$ orbital is Mo–Mo σ/δ in character[24] and is the only occupied metal-based orbital, such that the dimer can be considered d^1–d^1 (Mo(+5)) with a Mo–Mo single bond. The other six metal-based orbitals ($7b_u$–$8b_u$) are all destabilized by μ-S and S_t π-donation.

This interpretation of the bonding in *trans*-**1** contrasts with that obtained by Tyler et al. using the Xα–SW method.[21] They reported that the four highest occupied orbitals were the Cp-based Mo–Cp bonding interactions, with the Mo–Mo bonding orbital lying ~1 eV lower in energy. Similar abnormally high-energy metal–Cp interactions have been observed in related systems by the Xα–SW method.[25] This problem appears to be quite general when the Xα–SW method is applied to complexes containing metal–ligand π interactions.[26-28] While Tyler et al. provide a reasonable explanation for the observed photochemistry within the framework of their calculations, it must be acknowledged that there are differences between the Fenske–Hall and Xα–SW descriptions of the highest orbitals in these systems. These differences are currently under investigation.

As shown in Scheme I, the geometric isomerization from *trans*-**1** to **2** would involve the intermediacy of the unobserved tetrasulfido-bridged structure. This conformation can be achieved by simply rotating the two terminal sulfido ligands of *trans*-**1** into positions above and below the Mo–Mo vector and likewise rotating the Cp ligands until their centroids lie along the Mo–Mo vector (step a). The C_{2h} symmetry can be maintained throughout this process. The fate of the frontier orbitals during this isomerization can be traced with the Walsh diagram in Figure 2. A number of effects induced by this transformation are noteworthy: (i) The Mo–Mo σ-bonding orbital ($6a_g$) remains relatively unaffected. (ii) A sulfido lone-pair orbital ($4b_g$) is destabilized such that it becomes the LUMO of the $(\mu\text{-S})_4$ structure. (iii) The empty metal-based $4a_u$ orbital loses its S_t antibonding character and becomes the HOMO of the $(\mu\text{-S})_4$ species. Although the $(\mu\text{-S})_4$ intermediate would formally be considered a d^1–d^1 dimer containing Mo(+5), the above-memtioned orbital crossing results in a two-electron oxidation of the sulfido ligand set and a concomitant

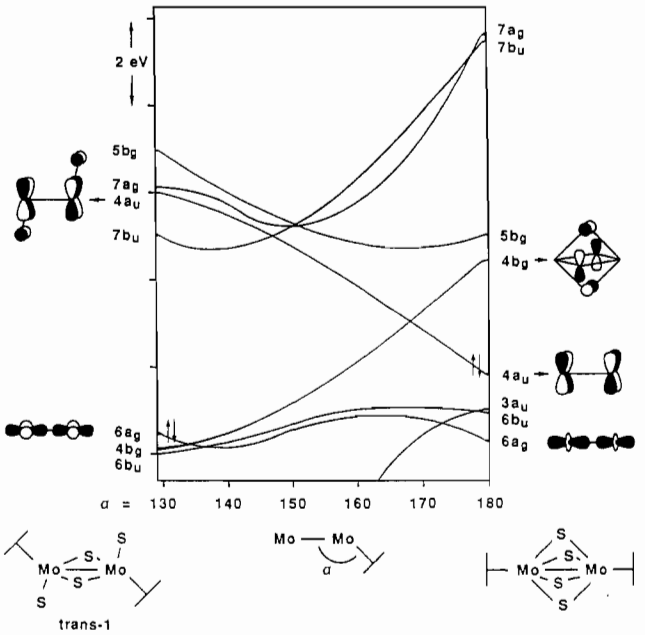

Figure 2. Walsh diagram depicting the variations in frontier orbital energies according to step a of Scheme I. The angle, α, refers to the Mo–Mo–Cp(centroid) angle.

reduction of the metal centers to Mo(+4). The fact that a $(\mu\text{-S})_4$ isomer of the $Cp_2Mo_2S_4$ system has never been observed appears to be due to the strong S–S antibonding interaction caused by bridging all four sulfido ligands. This unfavorable interaction manifests itself most clearly in the ligand-based $4b_g$ orbital. The μ-S p orbitals in the $4b_g$ orbital are all aligned in a mutually antibonding fashion, causing this "lone pair" to be destabilized to such a degree that it is a virtual orbital. DuBois and co-workers, employing the EHMO method, also found the $(\mu\text{-S})_4$ geometry to be unstable with respect to the $(S_t)_2(\mu\text{-S})_2$ (*trans*-**1**) geometry.[11] It is interesting, though, that the tetrabridged core geometry is the structure adopted by the closely related bis- and tetrakis(thiolato) piano-stool dimers $Cp_2Mo_2(\mu\text{-S})_2(\mu\text{-SR})_2$ and $Cp_2Mo_2(\mu\text{-SR})_4$.[11,19] This would, however, be consistent with our analysis since the coordination of alkyl groups to the sulfur ligands would remove the lone-pair–lone-pair antibonding interactions inherent within the naked sulfido bridges.

An alternative way to relieve the lone-pair–lone-pair repulsion in the $(\mu\text{-S})_4$ geometry is to form a S–S bond between two cis-sulfido bridging ligands. This route contains two stabilizing features: (i) Two of the former lone-pair–lone-pair interactions manifest themselves in S–S bonding and antibonding orbitals. (ii) The two μ-S ligands not involved in S–S bonding have room to move away from one another, hence minimizing their lone-pair–lone-pair repulsions. A view of this transformation down the Mo–Mo vector is provided in B to illustrate this effect. The

B

variations in frontier orbital energies along this isomerization coordinate (step b of Scheme I) are depicted in Figure 3. The symmetry of the $(\mu\text{-S})_4$ species on the left side of the diagram was altered from C_{2h} (as in Figure 2) to C_{2v} since that is the highest symmetry possible for this isomerization step. The differences in energies and compositions of the orbitals of the $(\mu\text{-S})_4$ species in either C_{2h} or C_{2v} symmetry are essentially negligible. In other words, rotation of either the Cp or the $(\mu\text{-S})_4$ ligands about the Mo–Mo vector causes little change in the overall electronic structure. The orbitals in Figure 3 that are most affected by the isomerization are, not surprisingly, the ligand-based orbitals. The $6b_1$ and $7b_1$ orbitals mix such that $7b_1$ correlates with the high-energy empty S–S σ^* interaction of the $\mu\text{-}S_2$ moiety, and $6b_1$

(24) Bursten, B. E.; Cayton, R. H.; Gatter, M. G. *Organometallics* **1988**, *7*, 1349–1356.
(25) Cayton, R. H. Unpublished results.
(26) Cotton, F. A.; Stanley, G. G.; Cowley, A. H.; Lattman, M. *Organometallics* **1988**, *7*, 835–840.
(27) Bursten, B. E.; Cotton, F. A.; Cowley, A. H.; Hanson, B. E.; Lattman, M.; Stanley, G. G. *J. Am. Chem. Soc.* **1979**, *101*, 6244–6249.
(28) Bursten, B. E.; Cotton, F. A.; Cowley, A. H.; Lattman, M.; Stanley, G. G. Unpublished Xα–SW and PES results.

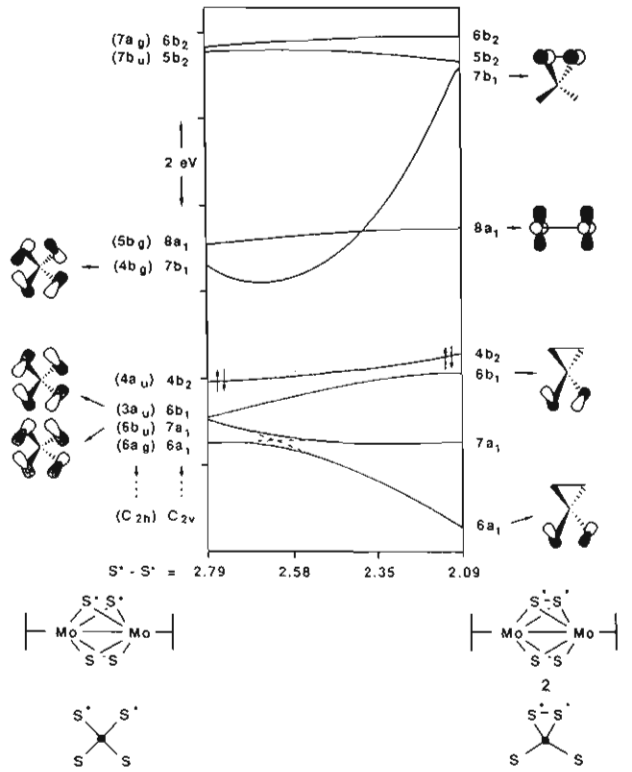

Figure 3. Walsh diagram depicting the variations in frontier orbital energies according to step b of Scheme I.

becomes an out-of-phase lone-pair combination on the two μ-S ligands. The $7a_1$ orbital undergoes an avoided crossing with the $6a_1$ Mo–Mo σ-bonding orbital as it correlates with the μ-S in-phase lone-pair combination. No filled–empty orbital crossings take place, and the metal centers remain formally d^2–d^2 (Mo(+4)).

It is interesting to note that although **2** is a d^2–d^2 dimer, and the HOMO is the metal-based $4b_2$ orbital, it appears that isomer **2** could accommodate another electron pair. The LUMO of **2** is the Mo-based $8a_1$ orbital, which is Mo–Mo δ in character and contains little sulfido character. In addition, the $8a_1$ orbital is energetically separated by >3.7 eV from the next lowest unoccupied orbital. Hence, through either the chemical or electrochemical reduction of $Cp^*_2Mo_2S_4$ or the replacement of Mo with a group VII metal, a d^3–d^3 species of structure type **2** may result.

We are now in a position to view the isomerization process from *trans*-**1** to **2** (steps a and b) in its entirety. The major consequence of this process is the transformation of a virtual Mo–S antibonding orbital into a purely Mo-based orbital, thus stabilizing it and occupying it with two electrons. The two electrons were taken from a S-based orbital that was destabilized as it became S–S antibonding. The net effect is a reduction of the metal centers and oxidation of two sulfido ligands, representing a thermally forbidden but photochemically allowed process. This is in agreement with the experimental observations.

Step c of Scheme I represents the one isomerization that was found to occur thermally. That this process should be allowed thermally is quite apparent from the Walsh diagram in Figure 4. The three highest occupied orbitals of **2**, $7a_1$, $6b_1$, and $4b_2$, correlate with occupied orbitals in **3**. The $7a_1$ and $4b_2$ orbitals are metal-based, Mo–S nonbonding orbitals. In **2** these orbitals represent Mo–Mo σ ($7a_1$) and δ^* ($4b_2$) interactions; however, in **3** they have rehybridized to form σ/δ ($7a_1$) and σ^*/δ^* ($4b_2$) combinations. This hybridization serves to somewhat weaken the Mo–Mo bonding as evidenced by the slight destabilization of the $7a_1$ orbital. It is also evident that a substantial HOMO–LUMO separation is maintained throughout the transformation. The metal-based Mo–S antibonding orbitals of **2** retain their sulfido antibonding character during the isomerization and remain unfilled and high in energy, consistent with the process being thermally allowed.

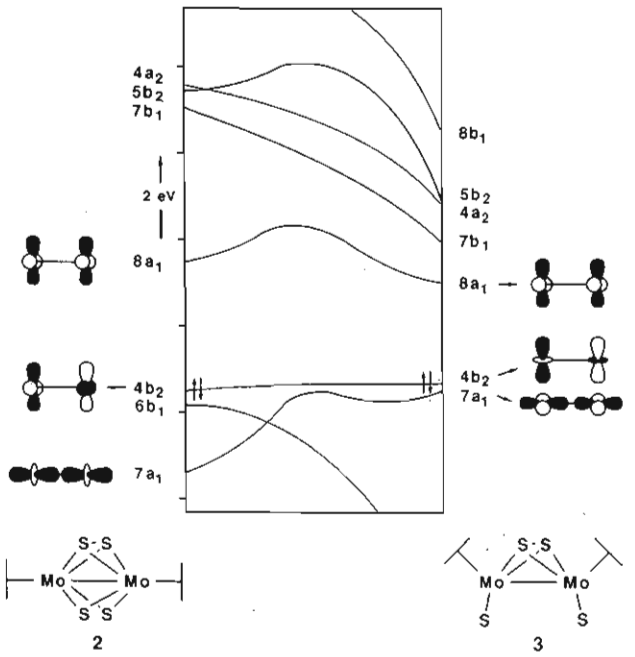

Figure 4. Walsh diagram depicting the variations in frontier orbital energies according to step c of Scheme I.

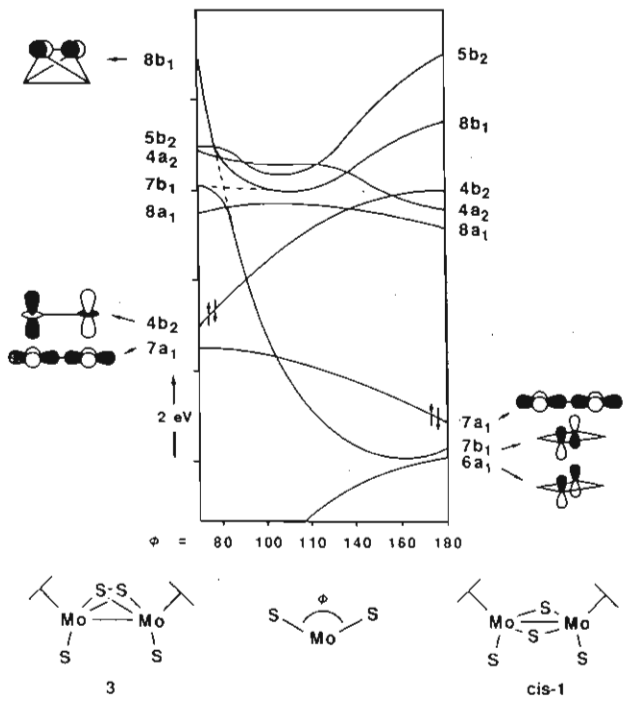

Figure 5. Walsh diagram depicting the variations in frontier orbital energies according to step d of Scheme I.

Although the existence of step d in the postulated isomerization mechanism of Scheme I has no experimental support, we thought it important to include in our theoretical investigation inasmuch as it represents a route to the cis isomer of **1**, and since the geometric transformation involved will be directly applicable to the forthcoming discussion of the tetraoxo analogues. The variation in orbital energies for this process is depicted in Figure 5. The angle ϕ represents the dihedral angle between the two Mo–(μ-S)–Mo bridge planes. The Mo(+4) centers of **3** are formally oxidized to the (+5) oxidation state in *cis*-**1**, and such is reflected in the Walsh diagram. The occupied Mo–S nonbonding $4b_2$ orbital of **3** is destabilized as the μ-S ligands are rotated down into a plane containing the Mo atoms and correlates to an empty Mo–S antibonding orbital in *cis*-**1**. The origin of this antibonding sulfido character is illustrated below. The two

electrons removed from the $4b_2$ orbital are transferred to the ligand-based $7b_1$ orbital, thus affecting a formal reduction of the μ-S ligands and oxidation of the Mo centers. The $7b_1$ and $8b_1$ orbitals of **3** undergo an avoided crossing such that the S–S σ^* character of $8b_1$ ultimately correlates with the μ-S nonbonding character in $7b_1$ of *cis*-**1**, as shown in C. The resulting electronic

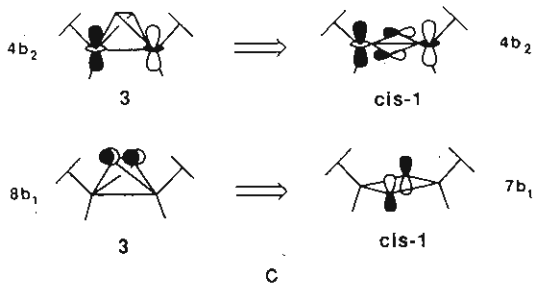

C

structure of *cis*-**1** is very similar to that already discussed for *trans*-**1**. Similar close relationships between the electronic structures of cis and trans isomers of low-valent $Cp_2M_2L_4$ systems have been observed previously.[24] As in *trans*-**1**, the HOMO ($7a_1$) is a Mo–Mo σ/δ interaction, with two nonbonding sulfido lone-pair orbitals located only slightly lower in energy. The HOMO–LUMO separation is also very similar in the two isomers (cf. *trans*-**1**, 4.62 eV; *cis*-**1**, 4.73 eV).

At this point it will be instructive to review the calculated potential surface modeling the isomerization of $Cp^*_2Mo_2S_4$. The pathway postulated in Scheme I appears consistent with the experimental observations. The calculations indicate that the transformation of isomer **1** to either **2** or **3** is only allowed photochemically, and the $(\mu\text{-S})_4$ transition state represents an unstable conformation. Moreover, the **2** $\rightleftarrows$ **3** isomerization was found to be thermally allowed. As far as reactivity is concerned, treatment of $Cp_2Mo_2S_4$ with H_2 results in the formation of a complex containing two sulfido bridges and two SH bridges (eq 1). Other

$$Cp_2Mo_2S_4 + H_2 \rightarrow Cp_2Mo_2(\mu\text{-S})_2(\mu\text{-SH})_2 \qquad (1)$$

hydrocarbyl ligands such as alkyls, alkenyls, and alkynyls may also be introduced onto the sulfido ligands to yield analogous products.[11,29,30] Similar addition reactions have also been observed for other unsaturated organic moieties,[29,31] as well as for transition-metal fragments en route to heteronuclear metal cluster systems.[32-37] From the electronic structures of the three isomers **1**, **2**, and **3**, it would appear that **2** contains the features most conducive to such reactivity. In particular, the $6b_1$ orbital of **2** (see Figure 3) is filled, is high in energy, is sterically accessible, and is of the correct symmetry to interact with and back-donate electron density to empty π-type orbitals of potential reactants.

$Cp_2Mo_2O_4$

As early as 1964, Cousins and Green isolated a complex of the formula $Cp_2Mo_2O_4$ (**4**) from the photolysis of a chloroform solution of $[CpMo(CO)_3]_2$ in air.[38] This compound can be more conveniently prepared through either the oxidation of $CpMo(CO)_3H$[38] or the hydrolysis of $CpMoBr_4$[39] or $CpMoCl_4$.[40,41] The

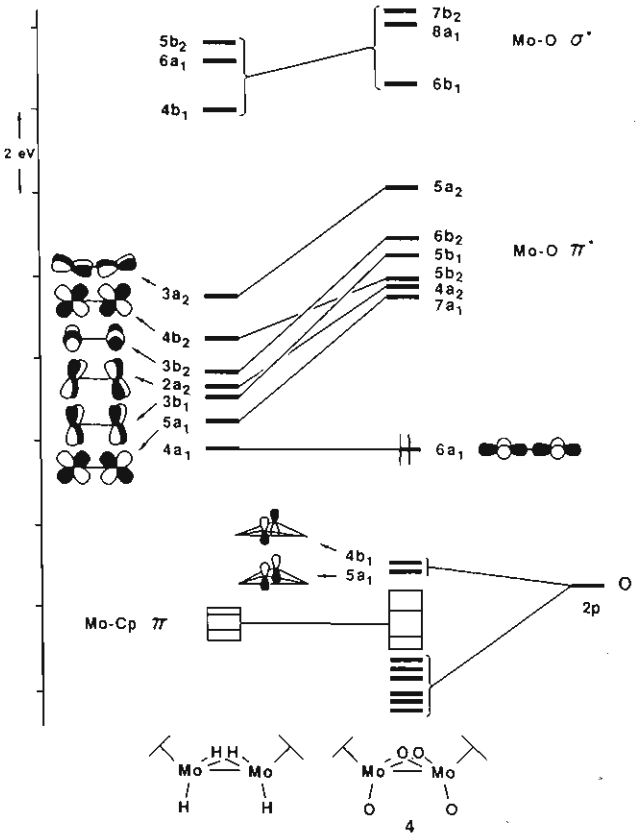

Figure 6. Frontier MO diagram of **4** showing its correlation to the orbitals of the σ-only framework *cis*-$[CpMoH]_2(\mu\text{-H})_2$.

structure of **4** was elucidated in 1978 as *cis*-$[CpMoO]_2(\mu\text{-O})_2$, containing two μ-oxo and two terminal oxo ligands, similar to *cis*-**1**.[7] One very interesting structural feature of **4** is its nonplanar Mo_2O_2 central core. The dihedral angle between the two Mo–(μ-O)–Mo planes is 154°, compared to 180° for the same angle in *trans*-**1**. The η^5-C_5Me_5 derivative has been prepared via the reaction of $[Cp^*Mo(CO)_2]_2$ with $(t\text{-BuNC})_2Ni(O_2)$, and its structure also exhibits a cis-Cp* geometry with a similar folding of the Mo_2O_2 core.[8] There has been no evidence to date for the existence of isomers of **4** displaying structures analogous to those observed for the sulfido species **2** and **3**. Hence, we sought to investigate the electronic structure and bonding in **4** in order to (i) compare the oxo and sulfido systems, (ii) examine the reasons behind the nonplanar Mo_2O_2 core, (iii) look at other possible geometric isomers of **4**, and (iv) comment on its possible reactivity patterns.

The frontier MO region of **4** is depicted in Figure 6, along with its correlation to the orbitals of the fictitious tetrahydrido (σ-only) framework *cis*-$[CpMoH]_2(\mu\text{-H})_2$. It is this σ-only framework that will ultimately provide the keys to understanding the puckered Mo_2O_2 core. First, however, let us compare the electronic structures of **4** and *trans*-**1**. Under C_{2v} symmetry, the eight oxo π orbitals transform as $2a_1 + 2a_2 + 2b_1 + 2b_2$. Six of these combinations find appropriate symmetry matches among the metal-based orbitals, leaving two ligand-based lone pairs ($5a_1$ and $4b_1$) as well as one metal-based orbital ($6a_1$) as metal–ligand nonbonding orbitals. Although the $5a_1$ and $6a_1$ orbitals are of the same symmetry, they do not interact because their overlap is negligible. As with *trans*-**1**, **4** is formally d^1–d^1 and two electrons are located in the Mo–Mo σ/δ bonding $6a_1$ orbital to provide a Mo–Mo single bond. It is interesting that the metal-based orbitals of **4** are not destabilized as greatly as the corresponding metal-

(29) DuBois, M. R.; VanDerveer, M. C.; DuBois, D. L.; Haltiwanger, R. C.; Miller, W. K. *J. Am. Chem. Soc.* **1980**, *102*, 7456–7461.
(30) DuBois, M. R.; Haltiwanger, R. C.; Miller, D. J.; Glatzmaier, G. *J. Am. Chem. Soc.* **1979**, *101*, 5245–5252.
(31) Miller, W. K.; Haltiwanger, R. C.; VanDerveer, M. C.; DuBois, M. R. *Inorg. Chem.* **1983**, *22*, 2973–2970.
(32) Brunner, H.; Wachter, J. *J. Organomet. Chem.* **1982**, *240*, C41–C44.
(33) Brunner, H.; Kauermann, H.; Wachter, J. *Angew. Chem.* **1983**, *95*, 567–568.
(34) Cowans, B.; Noordik, J.; DuBois, M. R. *Organometallics* **1983**, *2*, 931–932.
(35) Curtis, M. D.; Williams, P. D. *Inorg. Chem.* **1983**, *22*, 2661–2662.
(36) Brunner, H.; Kauermann, H.; Wachter, J. *J. Organomet. Chem.* **1984**, *265*, 189–198.
(37) Brunner, H.; Janietz, N.; Wachter, J.; Zahn, T.; Ziegler, M. L. *Angew. Chem.* **1985**, *97*, 122–123.
(38) Cousins, M.; Green, M. L. H. *J. Chem. Soc.* **1964**, 1567–1572.
(39) Cousins, M.; Green, M. L. H. *J. Chem. Soc. A* **1969**, 16–19.
(40) Bunker, M. J.; DeCian, A.; Green, M. L. H. *J. Chem. Soc., Chem. Commun.* **1977**, 59.
(41) Bunker, M. J.; Green, M. L. H. *J. Chem. Soc., Dalton Trans.* **1981**, 847–851.

based orbitals of *trans*-**1**. This feature manifests itself most notably in the larger HOMO–LUMO separation calculated for *trans*-**1** (4.62 eV) compared to **4** (3.85 eV). The stronger interaction of the Mo-based orbitals with the sulfido ligands compared to that with the oxo ligands is primarily due to the fact that the S 3p atomic orbitals lie 2.8 eV higher in energy than the O 2p atomic orbitals, hence, closer in energy to the Mo 4d orbitals. Another consequence of the lower energy O 2p orbitals is a lowering of the nonbonding oxo lone-pair set, $5a_1$ and $4b_1$ orbitals, 2.8 eV below the $6a_1$ HOMO of **4**. From their MO pictures, it would appear that **4** may be easier to oxidize than *trans*-**1** and, although comparative electrochemical studies have not been carried out, it has been found that solutions of **4** are readily air-oxidized or treated with Ag^+ to yield $[CpMoO_2]_2(\mu\text{-}O)$,[38,39,41] or oxidized with Br_2 to give $CpMoO_2Br$.[41]

The reasons for the puckered Mo_2O_2 core of **4** and the planar Mo_2S_2 core of *trans*-**1** can be rationalized through the orbital compositions of their respective σ-only bimetallic frameworks. The overall orbital descriptions of *cis*- and *trans*-$[CpMoH]_2(\mu\text{-}H)_2$ are, not surprisingly, quite similar. However, an important difference is evident in two related orbitals of each geometry. These are the $3b_g$ and $3a_u$ orbitals of the trans isomer (Figure 1) and the $3a_2$ and $2a_2$ orbitals of the cis isomer (Figure 6). These are pictured in D along with the (μ-L) in-plane, out-of-phase, π combination.

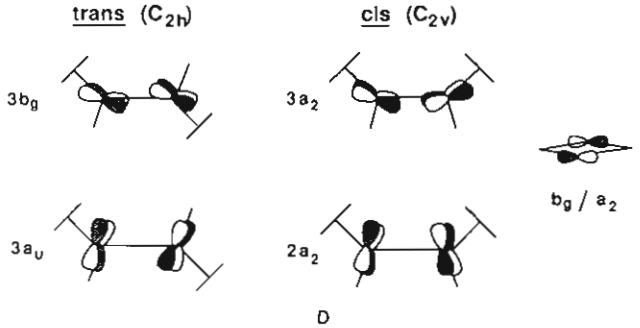

D

The ligand orbital transforms as b_g under C_{2h} symmetry and as a_2 under C_{2v} symmetry. Therefore, in *trans*-**1** the Mo_2S_2 core remains flat such that maximum overlap is achieved for this important b_g interaction. But in **4** the ligand a_2 combination has two metal-based a_2 orbitals to choose from, one "tilted" above the Mo–Mo vector ($2a_2$) and one below it ($3a_2$). The $2a_2$ orbital affords a better energy match with the ligand a_2 combination and, hence, dominates the bonding interaction, and since the $2a_2$ orbital is oriented on the "Cp side" of the molecule, the μ-O ligands are folded in that direction. It is interesting to note that in the *low-valent* complex *cis*-$[CpFe(CO)]_2(\mu\text{-}CO)_2$ the μ-CO bridges are folded *away* from the Cp ligands.[42] This is consistent with the above analysis since the CO π-back-bonding orbitals are empty, are high in energy, and would afford a better energy match with the metal-based $3a_2$ orbital. Thus, the $3a_2$ orbital would direct the μ-CO ligands to fold *away* from the "Cp side". This electronic effect has been observed previously in low-valent $Cp_2M_2L_4$ species by Hoffmann et al.[43]

The direction of the puckering of the Mo_2O_2 core of **4** places the structure along a distortion coordinate very similar to that examined in the **3** $\rightleftarrows$ *cis*-**1** isomerization (step d, Scheme I; Figure 5). Thus, we modeled a similar isomerization pathway for **4**, the results of which are shown in the Walsh diagram in Figure 7. Qualitatively, the orbital energy variations are quite similar to those of the sulfido system in Figure 5. It should be noted that as the dihedral angle between Mo–(μ-O)–Mo bridge planes (ϕ) is decreased from 180° (planar Mo_2O_2 core), the Mo–O antibonding $4a_2$ orbital is destabilized. This represents the enhanced Mo–O a_2 interaction in the lower bonding orbitals as a result of the greater overlap achieved by puckering the Mo_2O_2 core. As

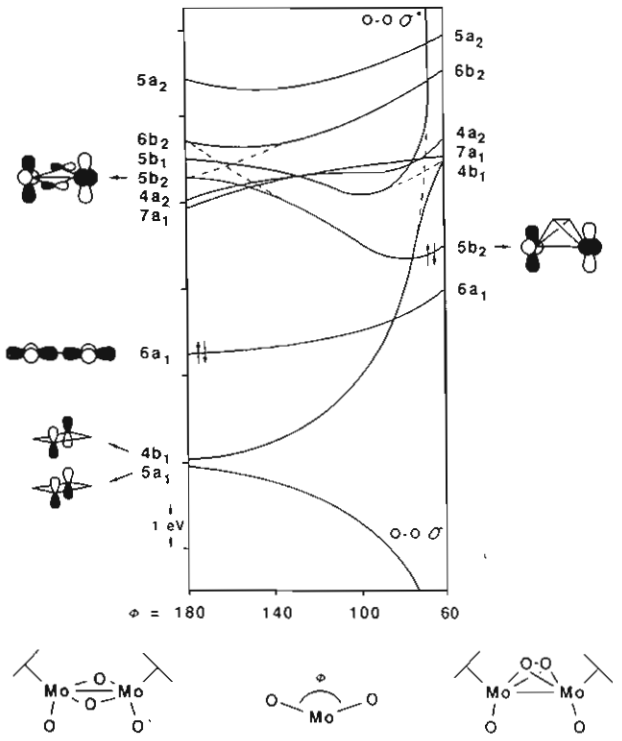

Figure 7. Walsh diagram depicting the variations in frontier orbital energies of *cis*-$[CpMoO]_2(\mu\text{-}O)_2$ with the angle ϕ.

the two μ-oxo ligands begin to approach one another, the two lone-pair orbitals, $5a_1$ and $4b_1$, begin to interact and ultimately correlate with a filled O–O σ and an empty O–O σ^* interaction, respectively. The two electrons removed from the $4b_1$ orbital are transferred to the metal-based $5b_2$ orbital, which is rendered Mo–O nonbonding as ϕ decreases. This filled-empty orbital crossing results in a formal reduction of the metal centers to Mo(+4) and concomitant oxidation of the bridging oxo ligands from $(\mu\text{-}O)_2^{4-}$ to $(\mu\text{-}O_2)^{2-}$. The orbital picture that develops for the d^2–d^2 μ-peroxo structure on the right side of Figure 7 appears stable. No Mo–O antibonding interactions are occupied, and a substantial HOMO–LUMO separation (2.2 eV) is achieved. Hence, prolonged photolysis of **4**, with the exclusion of O_2, may result in a peroxo derivative via the pathway described in Figure 7. It should be noted, however, that since the lone-pair orbitals $5a_1$ and $4b_1$ originate much lower in energy than the corresponding orbital set in *cis*-**1** (Figure 5), the calculated barrier for the conversion of **4** to the μ-peroxo species is 1.3 times greater than that calculated for the sulfido system. A final point of note concerning Figure 7 is that if the HOMO–LUMO separation is plotted against ϕ, it is found to maximize at $\phi \approx 155°$. That this value is close to that observed in the crystal structure of **4** may be fortuitous, but such correlations between HOMO–LUMO gap and stable conformations have been noted previously in similar systems.[18a,24,44–48]

Surprisingly, the reaction chemistry of **4** remains relatively unexplored, especially in view of the extensive chemistry that has been developed for *trans*-**1** and its derivatives. The two occupied lone-pair orbitals of **4** ($5a_1$ and $4b_1$) might be susceptible to electrophilic attack (e.g. protonation); however, their comparatively low energy may retard facile adduct formation analogous to that observed for $Cp^*_2Mo_2S_4$.

$Cp_2Re_2O_4$

It was shown earlier that the tetrasulfido Mo system undergoes facile interconversion between formally d^1–d^1 and d^2–d^2 bimetallic systems. The recent synthesis by Herrmann and co-workers of

(42) Bryan, R. F.; Greene, P. T.; Newlands, M. J.; Field, D. S. *J. Chem. Soc. A* **1970**, 3068–3074.
(43) Jemmis, E. D.; Pinhas, A. R.; Hoffmann, R. *J. Am. Chem. Soc.* **1980**, *102*, 2576–2585.
(44) Hofmann, P. *Angew. Chem.* **1977**, *89*, 551–553.
(45) Hofmann, P.; Padmanablan, M. *Organometallics* **1983**, *2*, 1273–1284.
(46) Bursten, B. E.; Gatter, M. G. *J. Am. Chem. Soc.* **1984**, *106*, 2554–2558.
(47) Bursten, B. E.; Gatter, M. G. *Organometallics* **1984**, *3*, 941–943.
(48) Bursten, B. E.; Cayton, R. H. *Organometallics* **1986**, *5*, 1051–1053.

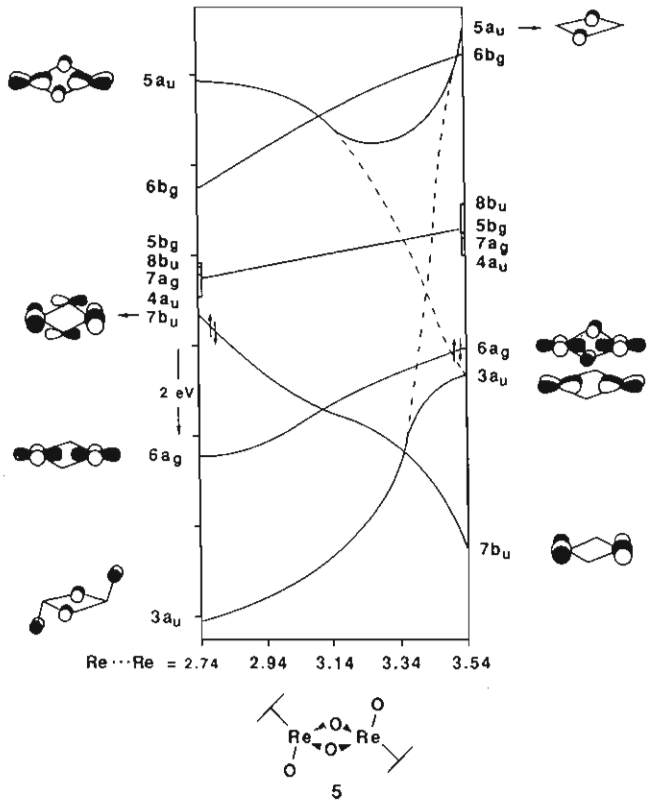

Figure 8. Walsh diagram depicting the variations in frontier orbital energies of *trans*-$[CpReO]_2(\mu\text{-}O)_2$ with Re–Re distance.

a d^2–d^2 analogue of the Mo dimer **4** allows a similar comparison to be made in the tetraoxo system. $[Cp^*ReO]_2(\mu\text{-}O)_2$ (**5**) was prepared via partial deoxygenation of Cp^*ReO_3 with PPh_3 and has been shown spectroscopically to contain two terminal and two bridging oxo ligands.[49-51] The solid-state structure of **5** has only recently been determined,[12] but before we detail its unique conformation it will prove interesting to examine its bonding based upon the electronic structure and geometry addressed earlier for the Mo system **4**. The electronic structure of **5** can be approximated by adding two electrons to **4**. From Figure 6 it is clear that such a reduction would result in the occupation of a high-energy metal–oxo antibonding orbital. However, the M–O antibonding character of this orbital can be removed if the compound distorts according to the potential surface illustrated earlier in Figure 7. At $\phi \approx 100°$, the $5b_2$ orbital becomes a metal-based antibonding orbital and a substantial HOMO–LUMO separation is generated. Any further decrease in ϕ would cause the deoccupation of a μ-oxo lone pair and occupation of a different high-energy metal–oxo antibonding orbital. Thus compound **5** could be expected to exhibit a cis-Cp* arrangement with an extremely puckered Re_2O_2 core ($\phi \ll 180°$). In fact, the closely related d^2–d^2 rhenium complex $[Cp^*(O)ReRe(OReO_3)_2Cp^*](\mu\text{-}O)_2$ does display such a folded Re_2O_2 core, with $\phi = 122°$.[50,52,53]

In contrast to the above conclusion, however, compound **5** exhibits a different, but equally fascinating, distortion to relieve the unstable core geometry associated with a M_2O_2 core analogous to that of **4**. In the crystal structure of **5**, the Cp* rings adopt a trans geometry, with a flat, but severely distorted, Re_2O_2 core. The Re–(μ-O)–Re angles average 106.7°, while the (μ-O)–Re(μ-O) angles average just 73.3°. For comparison, these same angles in **4** average 84.2 and 92.2°, respectively. This distortion affords a relatively long Re–Re distance of 3.14 Å and a somewhat short (μ-O)···(μ-O) distance of 2.34 Å (but not to the extent expected for a μ-peroxo structure). The stabilization incurred from this type of geometric perturbation can be understood with the aid of the Walsh diagram in Figure 8, which depicts the variations in orbital energies of **5** as the Re–Re distance is varied from 2.74 to 3.54 Å. As the Re–Re distance is increased, the occupied $7b_u$ orbital loses its Re–O antibonding character and is stabilized. At a Re–Re distance of 3.14 Å, both occupied metal-based orbitals ($7b_u$ and $6a_g$) are essentially Re–O nonbonding, but at larger Re–Re distances the $6a_g$ orbital begins to acquire Re–O antibonding character. Ultimately, at Re–Re = 3.54 Å, the μ-O ligands are close enough such that the $3a_u$ lone pair orbital correlates to an O–O σ^* ($5a_u$) orbital, and the system is formally reduced to d^3–d^3. Hence, the most stable Re_2O_2 core is that which is somewhere between a Re–Re bond and an O–O bond, and the dimer is held together through its Re–(μ-O) interactions. Table I lists the Fenske–Hall total energy,[54] HOMO energy, and HOMO–LUMO separation for **5** along the distortion coordinate detailed in Figure 8. Each of these three criteria favor the Re–Re distance of 3.14 Å, consistent with the solid-state structure.

Table I. Variations in Relative Total Energies, HOMO Energies, and HOMO–LUMO Separations in **5** with Respect to the Re–Re Distance

	Re–Re, Å				
	2.74	2.94	3.14	3.34	3.54
total energy (rel), (eV)	5.1	3.3	0.0	9.9	67.0
HOMO energy, eV	−7.22	−8.34	−8.74	−8.30	−8.02
HOMO–LUMO sepn, eV	0.43	1.67	2.26	2.04	2.12

Compound **5** undergoes some very interesting reaction chemistry and serves as the starting material in the preparation of numerous organometallic oxo complexes.[50,51] Many of these products appear to result from the initial cleavage of **5** into two $[Cp^*ReO_2]$ fragments. This is consistent with the electronic structure of **5** since the electron configuration is $(\sigma/\delta)^2(\sigma^*/\delta^*)^2$ and there is no net Re–Re bond. In addition, **5** can be protonated with 2 equiv of HBF_4 in Et_2O to yield the bis(hydroxo)-bridged dimer $[Cp^*ReO]_2(\mu\text{-}OH)_2^{2+}$.[50] This reaction may be considered as either an electrophilic addition to the filled μ-O orbitals, or as a charge-controlled attack of the protons on the most negative sites, namely the μ-O ligands.

One final point of interest concerning the structure of **5** involves the asymmetry associated with the Re–Cp* bonding. In the crystal structure of **5**, it is clear that the Cp* ligands are "slipped" in such a way that they are moved away from the O_t ligand, as shown in E. Similar "slipped" Cp* ligands have been observed in the

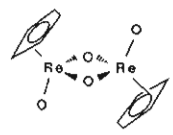

5

E

structures of other piano-stool complexes containing just one terminal oxo ligand.[55] Calculations performed on **5**, wherein a symmetric Re–Cp interaction has been assumed, show it to be 9.8 eV higher in energy than that with a "slipped" Cp ring. The destabilization associated with a "normal" Re–Cp interaction in **5** appears to be the result of an unfavorable filled–filled interaction between a Cp π orbital and a terminal oxo lone pair. This filled–filled interaction is minimized by sliding the Cp ligand away from the terminal oxo ligand as illustrated in F. Other ligands containing lone-pair electrons do not affect the M–Cp bond lengths

(49) Herrmann, W. A.; Serrano, R.; Bock, H. *Angew. Chem., Int. Ed. Engl.* **1984**, *23*, 383–385.
(50) Herrmann, W. A. *J. Organomet. Chem.* **1986**, *300*, 111–137 and references therein.
(51) Herrmann, W. A.; Herdtweck, E.; Floel, M.; Kulpe, J.; Kusthardt, U.; Okuda, J. *Polyhedron* **1987**, *6*, 1165–1182 and references therein.
(52) Herrmann, W. A.; Serrano, R.; Kusthardt, U.; Ziegler, M. L.; Guggolz, E.; Zahn, T. *Angew. Chem.* **1984**, *96*, 498–500; *Angew. Chem., Int. Ed. Engl.* **1984**, *23*, 515–517.
(53) Herrmann, W. A.; Serrano, R.; Kusthardt, U.; Guggolz, E.; Nuber, B.; Ziegler, M. L. *J. Organomet. Chem.* **1985**, *287*, 329–344.
(54) Batt, R. H.; Bursten, B. E.; Luth, K. W. Unpublished results.
(55) Hall, M. B.; Fenske, R. F. *Inorg. Chem.* **1972**, *11*, 768–775.

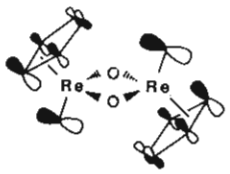

F

to the extent of the oxo ligand. For example, Cp^*ReOCl_2 displays a similar "slipped" Cp* ring, *toward* the Cl ligands.[51] This effect can be attributed to the very short M–O bond lengths for terminal oxo ligands, thus forcing their lone pairs closer to the Cp* π orbitals.

Acknowledgment. We gratefully acknowledge Professor W. A. Herrmann for communication of results prior to publication.

Appendix

Molecular orbital calculations were performed on an IBM 3081-D computer system using the Fenske–Hall approximate MO method.[55] The atomic positions for *trans*-**1**,[11] **2**,[10] **4**,[7] and **5**[12] were taken from their crystal structures and idealized to C_{2h}, C_{2v}, C_{2v}, and C_{2h} symmetry, respectively. All η^5-C_5R_5 rings were modeled by using η^5-C_5H_5 rings. Local D_{5h} symmetry was invoked upon the cyclopentadienyl rings, and a C–H distance of 1.08 Å was used for each calculation. In step a of Scheme I the surface was modeled by varying the Mo–Mo–S_t and Mo–Mo–Cp(centroid) angles as well as the Mo–Mo and Mo–S distances in a linear fashion. In step b, the symmetric $(\mu\text{-S})_4$ core was transformed into that of **2** by varying the S–S distances linearly. In step c, the Mo–Mo–S_t and Mo–Mo–Cp(centroid) angles were varied linearly. In step d, the dihedral angle between the Mo–(μ-S)–Mo bridge planes, ϕ, as well as the Mo–Mo and Mo–S distances were varied linearly such that the atomic positions in *cis*-**1** were the same as in *trans*-**1** after rotating one CpMoS fragment through 180° about the Mo–Mo vector. The potential surface illustrated in Figure 7 for compound **4** was generated by varying only the dihedral angle, ϕ, between the Mo–(μ-O)–Mo bridge planes. The potential surface modeled in Figure 8 was generated by varying the Re–Re distance from 2.74 to 3.54 Å and the (μ-O)···(μ-O) distance from 2.34 to 1.67 Å without varying any other bond lengths. The tetrahydrido frameworks used in Figures 1 and 6 were constructed from the interatomic angles of *trans*-**1** and **4**, respectively, by assuming the following bond lengths: Mo–H_t = 1.80 Å, Mo–(μ-H) = 1.90 Å.

All atomic wavefunctions were generated by using the method of Bursten, Jensen, and Fenske.[56] Contracted double-ζ representations were used for the Re 5d, Mo 4d, S 3p, C 2p, and O 2p AO's. An exponent of 1.16 was used for the H 1s AO.[57] The basis functions for Re and Mo were derived for the +3 oxidation state (s^0d^n) with the following fixed exponents: Re, 2.0 (6s), 1.8 (6p); Mo, 2.0 (5s), 1.6 (5p). For the C_5H_5 ligand, the first three occupied orbitals were filled with 2.0 electrons and deleted from the basis transformation set, and all virtual orbitals above the e_2'' level (D_{5h}) were filled with 0.0 electron and deleted from the basis transformation set in all calculations.[58] The C_5H_5 ligands were converged as the monoanion, the *molecular* orbitals of which were allowed to interact with the metal centers. All calculations were converged with a self-consistent-field iterative technique using a convergence criteria of 0.0010 as the largest deviation of atomic orbital populations between successive cycles.

(56) Bursten, B. E.; Jensen, J. R.; Fenske, R. F. *J. Chem. Phys.* **1978**, *68*, 3320–3321.
(57) Hehre, W. J.; Stewart, R. F.; Pople, J. A. *J. Chem. Phys.* **1969**, *51*, 2657–2664.
(58) Lichtenberger, D. L.; Fenske, R. F. *J. Chem. Phys.* **1976**, *64*, 4247–4264.

Contribution from the Istituto di Strutturistica Chimica "G. Giacomello", Area della Ricerca di Roma, CNR, C.P. 10, 00016 Monterotondo Stazione, Roma, Italy, and Istituto di Chimica, Università di Ferrara, via L. Borsari, 46, Ferrara, Italy

Stable Paramagnetic Dihydrido Complexes of Iridium(IV): Synthesis, X-ray Crystal Structure, and Behavior in Solution of $Ir^{IV}(H)_2(Cl)_2(P\text{-}i\text{-}Pr_3)_2$ (1) and $Ir^{IV}(H)_2(Cl)_2(PCy_3)_2$ (2)[1]

Pasquale Mura,* Annalaura Segre, and Silvana Sostero

Received October 17, 1988

The 17-electron dihydrido complexes of iridium(IV) $Ir^{IV}(H)_2(Cl)_2(P\text{-}i\text{-}Pr_3)_2$ (**1**) and $Ir^{IV}(H)_2(Cl)_2(PCy_3)_2$ (**2**) are prepared by the reaction of $(NH_4)_2IrCl_6$ with PR_3 (PR_3 = P-*i*-Pr_3 and PCy_3) in refluxing ethanol, containing concentrated HCl. Their magnetic moments are 1.5 and 1.6 μ_B, respectively. The crystal structures of **1** and **2** reveal slightly distorted octahedral geometries with three pairs of trans ligands: PR_3, Cl, and H. Contrary to all expectations, **1** and **2** give sharp, well-resolved ^1H NMR spectra in $CDCl_3$ solutions with hydride chemical shifts at extremely high field (δ = −49.0 (t) and −47.9 (t) ppm, respectively). A very unusual temperature-dependent solution equilibrium between paramagnetic and diamagnetic species involving molecular hydrogen is proposed for both complexes.

Introduction

Very few paramagnetic hydrides of transition metals are known,[2] and most of them, due to poor stability, have been characterized only in solution at low temperature by electron spin resonance spectroscopy.[3,4] To our knowledge, only two mononuclear tantalum[4] complexes, one cobalt[5] complex, and one binuclear rhodium[6] complex were sufficiently stable to allow the determination of their X-ray crystal structures.

Paramagnetic iridium(IV) complexes are stable and have been extensively investigated.[7] Furthermore, iridium easily forms hydrido compounds in the formal oxidation states I, III, and V.[8,9] Recently we reported the synthesis, X-ray crystal structure, and solution behavior of the first example of a paramagnetic hydrido

* To whom correspondence should be addressed at the Istituto di Strutturistica Chimica "G. Giacomello".

(1) Presented in part at the 3rd International Conference on the Chemistry of the Platinum Group Metals, Sheffield, U.K., July 13, 1987, and at the 20th Congresso Nazionale di Chimica Inorganica, Pavia, Italy, Sept 15, 1987.
(2) (a) Rhodes, L. F.; Zubkowski, J. D.; Folting, K.; Huffman, J. C.; Caulton, K. G. *Inorg. Chem.* **1982**, *21*, 4185–4192 and references cited therein. (b) Rhodes, L. F.; Caulton, K. G. *J. Am. Chem. Soc.* **1985**, *107*, 259–260 and references cited therein.
(3) Allison, J. D.; Walton, R. A. *J. Am. Chem. Soc.* **1984**, *106*, 163–168 and references cited therein.
(4) Luetkens, M. L., Jr.; Elcesser, W. L.; Huffman, J. C.; Sattelberger, A. P. *Inorg. Chem.* **1984**, *23*, 1718–1726 and references cited therein.
(5) Bianchini, C.; Masi, D.; Mealli, C.; Meli, A.; Sabat, M. *Gazz. Chim. Ital.* **1986**, *116*, 201–206.

0020-1669/89/1328-2853$01.50/0